How to cite: *Angew. Chem. Int. Ed.* **2022,** *61,* e202208436
International Edition: doi.org/10.1002/anie.202208436
German Edition: doi.org/10.1002/ange.202208436

Supramolecular Polymers | Hot Paper

Luminescence and Length Control in Nonchelated d^8-Metallosupramolecular Polymers through Metal-Metal Interactions

*Jonas Matern, Iván Maisuls, Cristian A. Strassert, and Gustavo Fernández**

Abstract: Supramolecular polymers (SPs) of d^8 transition metal complexes have received considerable attention by virtue of their rich photophysical properties arising from metal-metal interactions. However, thus far, the molecular design is restricted to complexes with chelating ligands due to their advantageous preorganization and strong ligand fields. Herein, we demonstrate unique pathway-controllable metal-metal-interactions and remarkable ^{3}MMLCT luminescence in SPs of a nonchelated Pt^{II} complex. Under kinetic control, self-complementary bisamide H-bonding motifs induce a rapid self-assembly into non-emissive H-type aggregates (**1A**). However, under thermodynamic conditions, a more efficient ligand coplanarization leads to superiorly stabilized SP **1B** with extended Pt···Pt interactions and remarkably long ^{3}MMLCT luminescence (τ^{77K} = 0.26 ms). The metal-metal interactions could be subsequently exploited to control the length of the emissive SPs using the seeded-growth approach.

Introduction

Supramolecular polymers (SPs)[1] of transition metal complexes have recently gained considerable attention due to their versatile self-assembly behavior and outstanding photophysical properties.[2] Particularly, the ability of self-assembled square-planar d^8 metal complexes to emit from triplet excited states, i.e., phosphorescence, is advantageous for a variety of applications, ranging from bioimaging[3] and photocatalysis[4] to active materials in photodynamic therapy,[5] OLEDs[6] and optical sensors,[7] among many others.[8,9] Especially in the case of heavy metals such as platinum, the spin-orbit coupling effect is beneficial to realize efficient intersystem crossing to access triplet excited states, from which the otherwise spin-forbidden phosphorescence becomes partially allowed.[10]

A remarkable feature of self-assembled d^8 metal complexes is their ability to develop metal-metal contacts through the interaction of the filled metal d_{z^2}-orbitals.[8,9] These interactions drastically affect the photophysical properties of the self-assembled materials and enable new electronic transitions, such as absorption of light into low-energy metal-metal-to-ligand charge transfer (MMLCT) states, from which luminescence can proceed.[4,7,11–22] A common strategy to enforce metal-metal-interactions and modulate the emission properties relies on the use of chelating, polydentate and/or cyclometalating aromatic ligands (Scheme 1a, top).[23] Their planar, preorganized π-surface facilitates the establishment of aromatic interactions into extended one-dimensional (1D) structures. The rigid aromatic scaffold furthermore minimizes the structural distortion of the excited states, reducing the rate constant of non-radiative decays (k_{nr}), which is directly linked to achieving high photoluminescence quantum yields (Φ_L) and long excited state lifetimes (τ).[10] Moreover, the generally strong σ-donor and π-acceptor character of these ligands raises the energy of otherwise thermally accessible, non-emissive metal-centered states, thus enhancing the emission properties.[10]

While ligand-unsupported metal-metal interactions have been reported for linear d^{10} systems,[24] MMLCT luminescence arising from extended metal-metal contacts has not yet been accomplished for SPs of d^8 complexes where no chelation is involved (Scheme 1a, bottom). This can be explained by the structural deviation from the ideal square-planar geometry and the tendency of monodentate aromatic ligand scaffolds to be arranged in a non-coplanar fashion with respect to the MX_2L_2 plane. For instance, commonly used pyridine ligands twist out-of-plane in crystal structures in order to avoid repulsive steric interactions between the pyridine α-protons and their neighboring ligands when coordinated in a square-planar geometry.[25] Moreover, monodentate acetylido (–C≡C–R) ligands, which possess a beneficial strong ligand field splitting, are commonly combined with sterically demanding phosphane ligands that hinder metal-metal-interactions.[26]

[*] Dr. J. Matern, Prof. Dr. G. Fernández
Organisch-Chemisches Institut, Westfälische Wilhelms-Universität Münster
Corrensstraße 36, 48149 Münster (Germany)
E-mail: fernandg@uni-muenster.de
Dr. I. Maisuls, Prof. Dr. C. A. Strassert
CiMIC, SoN, Institut für Anorganische und Analytische Chemie, Westfälische Wilhelms-Universität Münster
Corrensstraße 28/30, 48149 Münster (Germany)
and
CeNTech, Westfälische Wilhelms-Universität Münster
Heisenbergstraße 11, 48149 Münster (Germany)

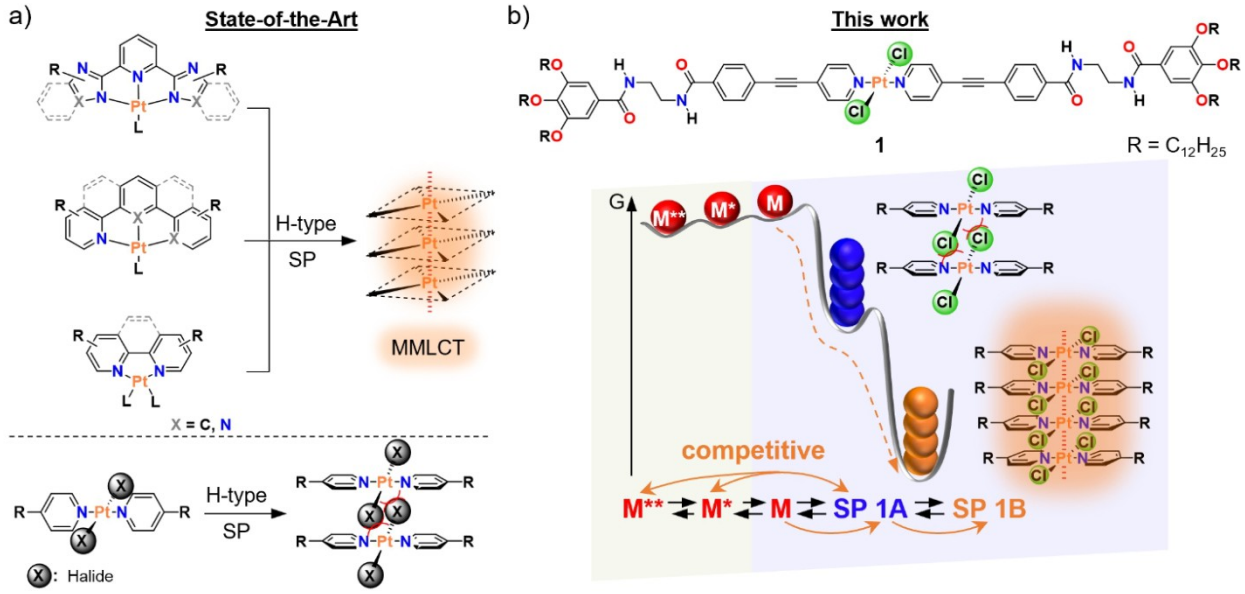

Scheme 1. a) State-of-the-art ligand design using polydentate ligands to achieve luminescent MSPs based on close Pt···Pt-contacts. b) Molecular structure and SP pathways of complex **1** investigated in this work leading to tunable MMLCT luminescence.

In this study, we demonstrate unprecedented luminescence and size control in SPs of a non-chelated d^8 complex via metal-metal interactions. To achieve this goal, we have designed a bispyridyldichlorido Pt^{II} complex **1** with an extended aromatic surface, decorated with two bisamide side groups and solubilizing dodecyloxy side chains (Scheme 1b). Contrary to literature reports, the bisamide linkers do not influence the SP by formation of metastable intramolecularly H-bonded pseudocycles, but they do induce pathway complexity:[27] Initially, the strong, highly directional H-bonding arrays prompt a rapid SP into kinetically controlled non-emissive H-type aggregates (**1A**). However, pathway control enables a consecutive transformation to the thermodynamic aggregate exhibiting close Pt···Pt contacts with long-lived ^{3}MMLCT emission (Scheme 1b). Our results demonstrate that the rational choice of aromatic and strong H-bonding interactions can counterbalance the inherent steric effects associated with the coordination of monodentate ligands to metal centers in a square-planar geometry, leading to ^{3}MMLCT emission upon SP.

Results and Discussion

Self-Assembly and Photophysical Properties

We identified apolar solvents such as *n*-hexane (*n*-Hex) and methylcyclohexane (MCH) as suitable solvents for self-assembly, while **1** is molecularly dissolved in typical "good" solvents (Figure S1). To explore the self-assembly in solution, variable-temperature (VT) absorption and emission studies were conducted. Due to the limited solubility of the self-assembled structures in pure apolar solvents, mixtures of MCH and chloroform ($CHCl_3$) were used (between 20–30 % v/v, Figure S2). Figure 1 shows the VT-UV/Vis absorption and emission spectra of **1** upon cooling at a rate of 1 K min^{-1}. Notably, the outcome of the self-assembly was observed to strongly depend on whether or not the solutions are stirred during the VT-studies.

Cooling without the influx of mechanical energy leads to a hypsochromic shift of the main absorption maximum from 312 nm to 298 nm, which is accompanied by the broadening of the shoulder band at ≈350 nm (aggregate **1A**, Figure 1a). In addition, a slight decrease in absorbance is observed when compared to higher temperatures. Emission studies reveal a practically non-emissive aggregate state (Figure 1a). Atomic force microscopy (AFM, Figure 1b) and scanning electron microscopy (SEM, Figure 1c) visualized **1A** in the form of flexible fibers (→SPs) with a strong propensity to form intertwined superstructures (Figures S3 & S4).

On the contrary, distinct spectroscopic changes occur when the solutions of **1** are stirred during cooling (formation of aggregate **1B**). The absorption spectra show a drop of the absorbance, accompanied by a hypsochromic shift of the absorption maximum to 292 nm, along with the rise of a second maximum at 327 nm and a shoulder between 345–375 nm (Figure 1d). Compared to the solution without stirring, the aggregate spectrum looks more defined and exhibits a more intense and sharper maximum at 270 nm, which is only visible as a shoulder without stirring. AFM and SEM studies of **1B** also revealed flexible SPs (Figure 1e,f & S5), albeit with a lower degree of random coiling and with a higher propensity for lateral alignment. At greater levels of magnification, a twist along the long axis of the fibers can be recognized, although no defined helicity is appreciable (see arrows in Figures 1e & S5e–g). In both SP **1A** and **1B**, interdigitation of the aliphatic side chains was identified to cause the bundling of the fibers, as evidenced

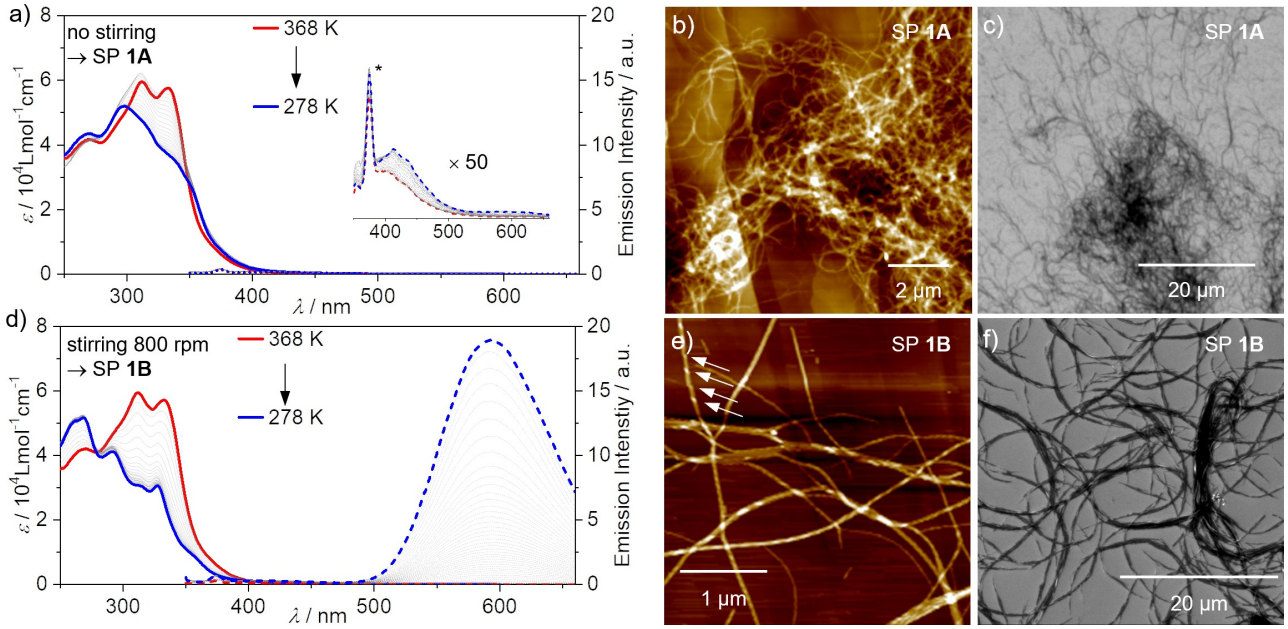

Figure 1. a), d) VT-UV/Vis absorption (solid lines, $c = 15\ \mu M$) and emission spectra (dashed lines, $c = 20\ \mu M$, $\lambda_{exc} = 333$ nm) upon cooling solutions of **1** (1 K min^{-1}, MCH:$CHCl_3$ 8:2). b), e) AFM images (HOPG). c), f) SEM images (silicon wafer) at 298 K. *Raman scattering peak.

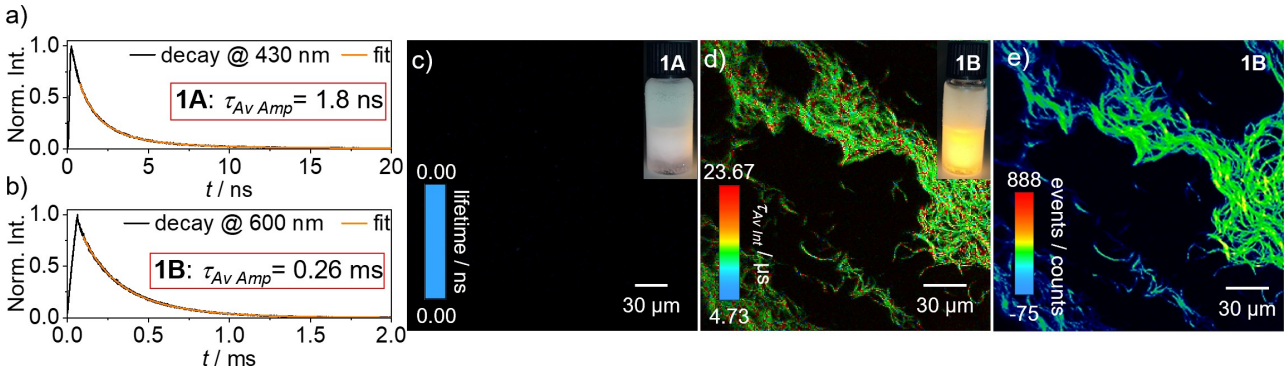

Figure 2. a), b) Time-resolved photoluminescence decay profiles of SP **1A** (a) and SP **1B** (b) at 77 K ($\lambda_{exc} = 325$ nm, MCH:$CHCl_3$ 8:2, $c = 20\ \mu M$). c)–e) Phosphorescence lifetime imaging (PLIM) studies ($\lambda_{exc} = 375$ nm, $T = 298$ K) with micrographs of the corresponding solutions under irradiation with an LED lamp ($\lambda_{exc} = 365$ nm). c) Photoluminescence lifetime map of SP **1A** showing the absence of emission. d) Photoluminescence lifetime map of SP **1B**. e) Micrograph of SP **1B** depicting detection events (photons that reach the detector, which correlates with the photoluminescence intensity).

from characteristic values of the CH_2 stretching vibrations of these groups in FTIR studies (Figure S5h).

The corresponding VT-emission studies monitoring the formation of **1B** show the progressive rise of an emission band at 593 nm upon cooling (Figure 1d). The large Stokes shift and the aggregation-induced enhanced emission behavior draw parallels to aggregates of other Pt^{II} complexes exhibiting close metal-metal contacts, giving rise to ^{3}MMLCT emission.[4,7,11–18,20–22] These results strongly suggest the formation of extended Pt···Pt-interactions in SP **1B**.

To corroborate this assumption, the emission properties of the different species of **1** were subjected to further characterization, both at room temperature (RT) and at 77 K (Figures 2 & S6–S8). The emission lifetimes of the monomers and SPs **1A** are below 2 ns, both at RT and at 77 K, characterizing the emission as fluorescence (Figures 2a, S6 & S7, $\lambda_{em} \approx 375$–500 nm). In stark contrast, the intense, red-shifted emission of SP **1B** at 593 nm showed a considerable increment in the photoluminescence lifetimes (Figures 2b & S8). At RT, the amplitude-weighted average photoluminescence lifetime was determined to be $\tau_{av\ amp} = 7.0 \pm 0.1$ μs, which is significantly increased to $\tau_{av\ amp} = 260 \pm 3$ μs at 77 K. This substantial increase in the lifetimes can be correlated with a luminescence process arising from a triplet state (→ ^{3}MMLCT). Interestingly, these lifetimes are longer than those determined for polydentate Pt^{II} aggregates or polymers found in the bibliography.[16,18,28] At 77 K, the emission quantum yield of SPs **1B** was determined to be $\Phi_L^{77\,K} = 0.53 \pm 0.02$ (for the quantum yields of all species at RT, see Figures S6–S8). The excitation spectrum collected

from the triplet emission of **1B** at $\lambda_{em} = 593$ nm furthermore allowed to assign the weak absorption at $\lambda = 355$ nm to the electronic transition into the ^{1}MMLCT excited state (Figure S8). Based on this experimental evidence, we conclude that **1** self-assembles into two distinct H-type SPs: **1A** lacking and **1B** exhibiting close Pt···Pt-interactions.

The remarkable emission properties of **1B** furthermore allowed us to apply emission lifetime-resolved imaging for the first time in the field of SPs as a technique orthogonal to conventional imaging methods such as AFM or SEM. This method simultaneously analyzes morphology, emission spectra and lifetimes, allowing to conclusively correlate these independent parameters without possible biases through different preparation protocols (e.g. discrepancies between solution and solid-state measurements). Phosphorescence lifetime imaging microscopy (PLIM) studies of the two aggregates (Figures 2c,d & S9) prove that both packing modes are preserved on solid substrates: Only the long-lived ^{3}MMLCT luminescence lifetimes give a clear picture of the aggregate fibers (Figure 2c,d). In the case of **1A**, no structures can be visualized as a result of the short fluorescence emission lifetimes (Figure S9).

Thermodynamic and Kinetic Analysis of the SP

Mechanistic insights into the SP of **1A** and **1B** were gained by monitoring the UV/Vis spectral changes as a function of temperature. In all cases, the data sets were extracted from cooling experiments at 1 Kmin^{-1}, starting from the monomer state at high temperatures (**1A**: no stirring, **1B**: 800 rpm). For both aggregates, plotting the development of the absorbance at $\lambda_{max} = 333$ nm vs. temperature yielded cooling curves that were fitted to the nucleation-elongation model (Figures 3a, S10 & S11).[29] The thermodynamic parameters derived from the fits (Table S1) demonstrate that **1B** is more stable (ΔG^{298}) than **1A** by ca. 15 kJ mol^{-1} and also exhibits a more cooperative character (σ). The extracted data also infers that prior to establishing Pt···Pt interactions in **1B**, a higher activation barrier has to be overcome ($\Delta H^{nucl.}$). This is also underlined by the fact that heating of kinetic **1A** first induces a **1A**→**1B** conversion before disassembly takes place (Figures 3b & S12). On the other hand, a direct disassembly occurs if aliquots of good solvent are gradually added to a solution of **1A** ("denaturation", Figure S13). While in the former experiment the initial thermal energy input helps to surpass the activation barrier for aggregate interconversion/formation of **1B**, the increasing volume fraction of good solvent merely increases the dynamics of the solution processes[14,30,31] and lowers the stability of all aggregated species at the same time. Thus, we conclude that **1A** is a non-transient species, i.e., a local minimum in the energy landscape of the SP of **1**.

The **1A**→**1B** transformation could be monitored by emission spectroscopy at RT after optimizing the experimental conditions (proper amount of $CHCl_3$, initial sonication & subsequent stirring, Figures 3c,d & S14, for details, see the Supporting Information). Notably, the transformation is slightly faster at higher concentrations, indicative of an on-pathway, consecutive transformation.[32] The initially more pronounced increase of the emission intensity (≈0–200 min) and the subsequent levelling (≈200–500 min) could possibly be correlated to an initially greater number of SP strands, for which the transformation to SP **1B** was already initiated in the precedent sonication step. Once these strands have fully rearranged to SP **1B**, the continuous mechanical stirring can only induce a gradual transformation for residual **1A** SPs. Shortly tempering the solutions at 313 K for 5 min and subsequent continuation of the measurement at 298 K re-accelerates the transformation rate before it levels again after some time (Figure 3d). Hence, thermal energy input is also beneficial to overcome the activation barrier for a rearrangement of a larger number of SP strands, in line with the conclusions drawn from the disassembly studies upon heating.

Elucidation of Interactions and Packing Modes

To clarify the packing modes in the two SPs, combined ^{1}H NMR and FTIR studies were conducted. The FTIR spectra of monomers ($CHCl_3$) and of thin films of both aggregates are shown in Figure 4b. As previously reported, the spectrum of the molecularly dissolved state exhibits amide N–H

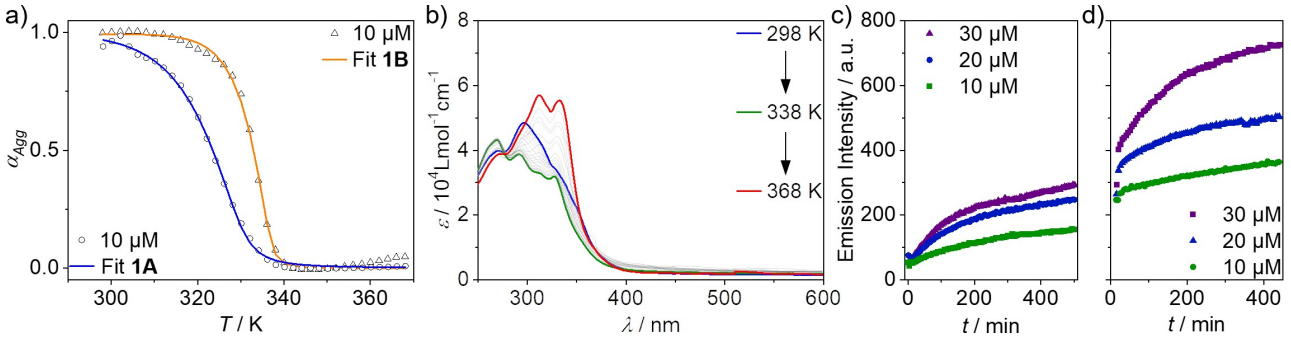

Figure 3. a) Cooling curves (1 Kmin^{-1}) and fits to the nucleation-elongation model for the self-assembly of **1A** (unstirred, blue) and **1B** (stirred, 800 rpm, orange). b) VT-UV/Vis spectra recorded upon heating a solution of SP **1A** (MCH:$CHCl_3$ 8:2, 1 Kmin^{-1}). c), d) Development of the emission intensity at λ_{max} in time-dependent emission studies of the **1A**→**1B** transformation upon stirring a solution of SP **1A** at 298 K (c), shortly tempering the solutions at 313 K and subsequently continuing the measurement at 298 K (d; MCH:$CHCl_3$ 7:3, 800 rpm, $\lambda_{exc} = 333$ nm).

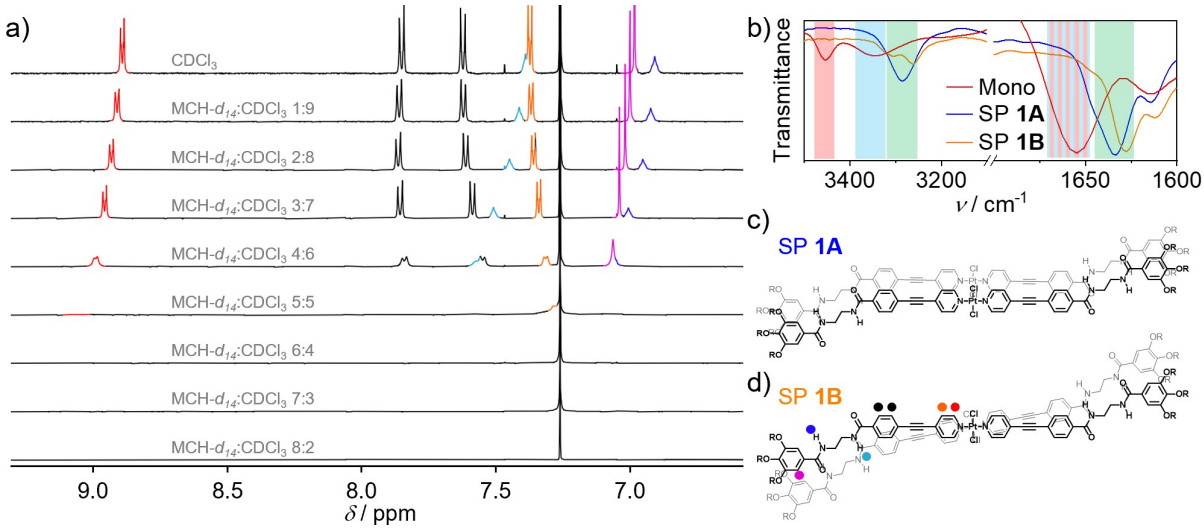

Figure 4. a) Partial ^{1}H NMR spectra monitoring the formation of SP **1B** upon increasing the MCH-d_{14}:$CDCl_3$ ratio (c = 1 mM, T = 298 K). b) Partial thin-film ATR-FTIR spectra of SP **1A** (blue) and SP **1B** (orange). The colored areas denote the regions of free (red), intra- (cyan) and intermolecularly (green) H-bonded amide groups. c), d) Proposed molecular arrangements of the complexes in the two SPs.

and C=O stretching bands characteristic for the equilibrium between open and intramolecularly H-bonded monomers (ν_{N-H} (free) = 3454 cm^{-1}, ν_{N-H} (intra) = 3348 cm^{-1}, $\nu_{C=O}$ (mixed) = 1655 cm^{-1}).[33] **1A** displays an N–H stretching band at ν_{N-H} = 3286 cm^{-1}, and a carbonyl stretching band at $\nu_{C=O}$ = 1633 cm^{-1} (Figure 4b), in accordance with the formation of intermolecular amide-to-amide H-bonds.[34,35] For SP **1B**, the carbonyl stretching band is further displaced to lower wavenumbers ($\nu_{C=O}$ = 1628 cm^{-1}), indicating marginally stronger H-bonding. The N–H stretching band splits into two bands at higher and lower wavenumbers (ν_{N-H} = 3262 cm^{-1}, 3305 cm^{-1}). Both values can be assigned to intermolecular H-bonds (compare ν_{N-H} (intra) ≈3350 cm^{-1}).[33,36]

The packing mode of **1B** was further characterized by ^{1}H NMR studies upon increasing the MCH-d_{14}/$CDCl_3$ ratio, starting from the monomeric state in pure $CDCl_3$ (Figure 4a & S15). Initially, the α-pyridine proton (red) shifts to lower fields, which is characteristic for a coplanarization of the pyridine ring with respect to the N–Pt–Cl plane, causing closer intramolecular Cl···H_α-pyridine contacts.[18] On the other hand, the resonances of the β-pyridine protons (orange) and the protons of the central aromatic ring (black) undergo upfield shifts, indicating aromatic interactions. Both amide proton resonances (blue + cyan) strongly deshield, in line with the formation of intermolecular amide-amide H-bonds. All these shifts are accompanied by a strong broadening at high MCH-d_{14} ratios, in agreement with the formation of polymeric assemblies. Based on these results (the same trends are observed in VT-NMR, Figure S16), we propose an H-type arrangement for both aggregates.

Despite the comparable intermolecular interactions for **1A** and **1B**, the subtle differences observed in FTIR studies indicate a slightly altered packing mode. For **1A**, the appearance of a single N–H stretching frequency suggests that all four amide groups engage into H-bonding interactions of comparable geometry and strength. This could be envisioned in a parallel stacking with a symmetrical alignment of the amide moieties (Figure 5c). In contrast, for **1B**, the coplanarization of the chlorido and pyridine ligands, which as such is sterically unfavorable, enables closer interactions of the metal centers, giving way to attractive Pt···Pt-interactions. This spatial approximation could induce a small rotational offset to minimize intermolecular steric repulsion in the metal's densely packed periphery (Figure 4d), resulting in a slightly altered H-bonding geometry for the inner vs. the outer amide groups. This hypothesis may explain the splitting of the N–H stretching band of **1B**. At the same time, the repulsive coplanarization could account for the higher activation barrier determined for **1B**. These findings are in line with the consecutive nature of the **1A**→**1B** transformation. After the initial formation of **1A**, only relatively minor rearrangements are required for **1B** to form. Moreover, the transfer of the rotational displacement in **1B** to the macroscopic level upon elongation could be the reason for the more twisted/helical morphology of **1B**.

Mechanistic Analysis of H-Bonding Interactions under Kinetic and Thermodynamic Control

Given that bisamide synthons are present in **1**, we next analyzed the influence of intra- and intermolecular H-bonds on the kinetically controlled SP.[34,35,37–39] Although **1** can effectively form intramolecular H-bonds in the monomers (see "c^1" and "c^2" conformations in Figure 5a and VT-^{1}H NMR in Figure S17), none of the two SPs incorporates intramolecular H-bonds. Kinetic studies on the SP into the all-intermolecularly H-bonded SP **1A** exhibit longer lag times at lower concentrations (Figures 5b & S18). Such a behavior is typical for the competitive formation of intramolecularly H-bonded monomers, whereas the growth of

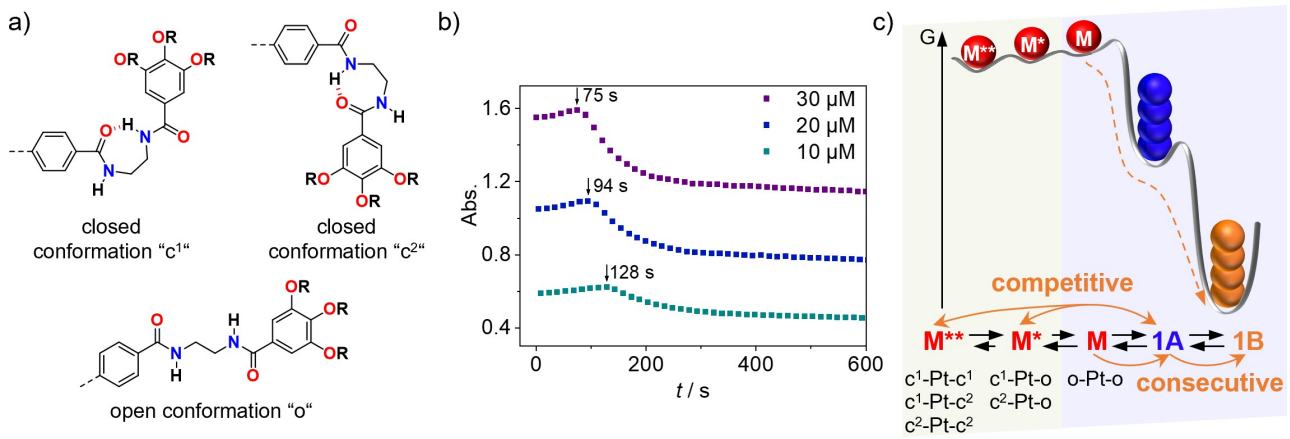

Figure 5. a) Possible conformations per bisamide moiety. b) Time-dependent UV/Vis studies of **1A** upon rapidly cooling a hot monomer solution from 368 K to 298 K ($\lambda = 333$ nm, MCH:$CHCl_3$ 8:2, $T = 298$ K). c) Energy landscape illustrating the SP of **1**. The abbreviations "*x*-Pt-*y*" listed below the monomer states denote the different conformers of **1**.

intermolecularly H-bonded SPs requires the open monomer conformation as feedstock ("o" in Figure 5a).[37,40] With this information, we were able to establish a qualitative energy landscape for the SP of **1** (Figure 5c).

Moreover, the self-assembly of **1A** is only marginally delayed (short lag times < 3 min), indicating an ineffective kinetic trap. This is especially surprising considering that the free ligand (precursor of complex **1**) undergoes a delayed SP due to the formation of two metastable species: Metastable c^1 and c^2 monomer conformers evolve into another metastable intermediate (dimer in which all H-bonding sites are saturated) before SP-elongation.[33] We hypothesize that various structural aspects are responsible for the different behavior of complex **1**. i) The free ligand is unsymmetrical and can hypothetically engage into a larger variety of packing modes (e.g. parallel and antiparallel).[33,41] ii) Complex **1** possesses a more pronounced aggregation propensity due to its larger π-surface and twice the number of H-bonding sites. iii) The complex has a higher conformational freedom, which disfavors kinetic trapping. Particularly, both bisamide motifs in **1** have to adopt a pseudo-cyclic conformation to achieve a "fully" SP-deactivated monomer state M** (→ in total six combinations of "o", "c^1" and "c^2" conformations per complex are possible, see Figure 5c & S19). Considering the dynamic equilibrium between open and pseudo-cyclic conformations, this is much less likely to occur compared to the ligand alone, for which two out of three conformations are "fully" SP-deactivated (Figure S19). Finally, the formation of a dimer of **1** cannot lock all H-bonding sites in a saturated conformation, leaving one amide unit prone for intermolecular association (Figure S20).

We thus infer that the evolution of the intermolecularly H-bonded SP **1A** under kinetic control requires only a minor preorganization of the monomers, causing a rapid growth of the H-bonding array, albeit with a lower degree of cooperativity. In contrast, under thermodynamic control, the H-bonds are conditioned by the evolution of metal-metal-interactions. This effect requires a previous coplanarization around the metal center to facilitate a closer approximation of the complexes. These prerequisites eventually cause a higher nucleation penalty for the SP into **1B** and, in turn, higher degrees of cooperativity (see Table S1).

Computational Studies

Theoretical calculations were performed to validate the conclusions drawn from the experimental data. The geometries of monomers to tetramers in a helical and a parallel packing were optimized in vacuum using the dispersion-corrected PM6 method (Figures 6, S21 & S22, for details, see the Supporting Information).

For the proposed parallel arrangement of **1A**, the calculations predict increasing Pt···Pt distances upon elongation (Table S2). This behavior can be attributed to the enhanced steric effects around the metal center as a result of a lower degree of coplanarization of the pyridine and chlorido ligands. This hypothesis is supported by the large θ (C–N–Pt–Cl) dihedral angles, which prevent an efficient approximation of the monomers in **1A**.

The optimizations of helical stacks to describe **1B** result in gradually decreasing θ (C–N–Pt–Cl) and Pt···Pt distances upon increasing the size of the stack to a trimer and tetramer (Table S3). Although the value of 3.81 Å obtained for the tetramer is still larger than the sum of the van der Waals radii of Pt (≈3.5 Å), extrapolation of the decreasing dihedral angles and Pt···Pt distances to an actual polymer is expected to result in closer Pt···Pt contacts. The N–H···O=C distances on the other hand are similar for **1A** and **1B**, indicating a comparable H-bonding strength. On this basis, we hypothesize that strong H-bonds enforce a parallel molecular arrangement in **1B**, but the simultaneous coplanarization and a slight rotational displacement enable a close approximation and interactions of the Pt^{II} centers.

We subsequently inspected the energy changes during di-, tri- and tetramerization. In agreement with the experimentally observed spontaneous formation of **1A**, the average stabilization energy per monomer (ΔE_{avg}) in a

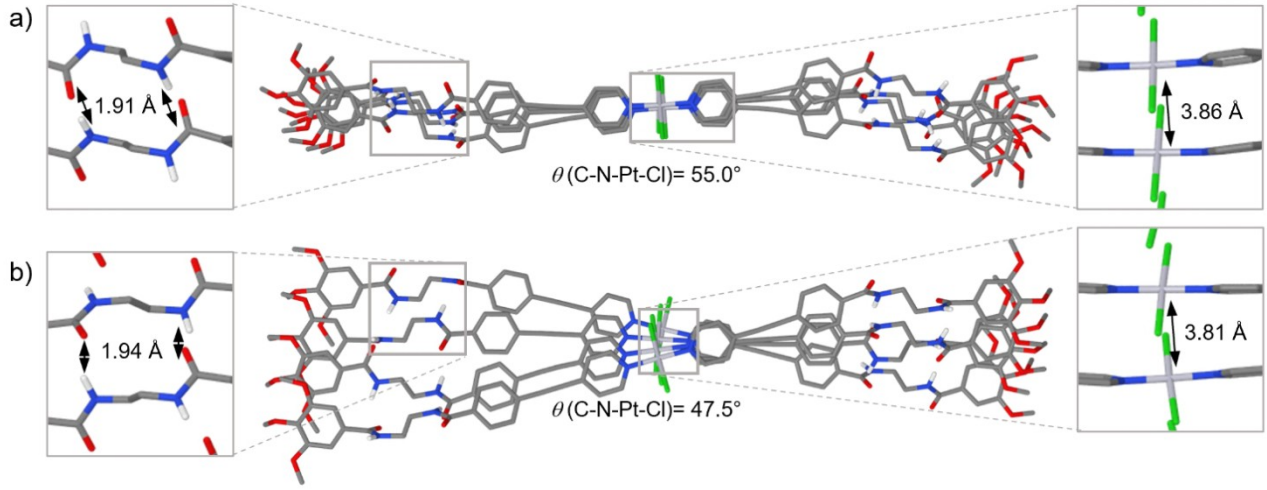

Figure 6. Dispersion-corrected PM6 geometry-optimized tetramers of **1** in a parallel (a) and a helical packing (b).

parallel arrangement becomes more negative during the initial association steps. In contrast, ΔE_{avg} slightly increases for **1B** up to the trimer and subsequently starts to become more negative, indicating a disfavored nucleation of **1B** compared to **1A**. However, the energy gain in an SP consisting of a much larger number of molecules is expected to be much greater for the helical arrangement than for the parallel one. These findings match well with the lack of spontaneous formation of SP **1B**, which on the other hand is energetically favored over formation of **1A** once nucleation of **1B** has occurred.

Living Supramolecular Polymerization (LSP): Pt···Pt-Interactions Drive H-Bonding Rearrangements

Delaying the formation of extended intermolecular H-bonds is a common approach to realize size control of SPs by means of seed-mediated approaches.[42,43] As the SP of **1** is not delayed by the competition between intra- and intermolecular H-bonds (see previous section), we probed whether metal-metal-interactions would be a sufficiently strong driving force to realize a seed-mediated living SP (LSP).[13,17,44,45] Upon the addition of **1B** seeds, kinetic **1A** was successfully transformed into **1B** within >12 h (Figure S23). To accelerate the dynamics in the solution, the volume fraction of good solvent was raised to 30 % v/v.[14,30,31] Figure 7 depicts the SP growth process in several cycles of adding kinetic **1A** to an invariant amount of **1B** seeds. Instantly after the first addition step, the ^{3}MMLCT emission starts to grow (Figure 7b). This behavior is characteristic for SPs formed in a nucleated process: The energy barrier for the nucleation of **1B**, which in the absence of seeds cancels the spontaneous **1A**→**1B** transformation (Figure S24), is overcome by the addition of seeds. In each cycle, the growth rate is attenuated by approximately half, revealing the living character of the process (Figure 7c).[43,46] The controlled, stepwise increase in the length of the aggregates (Figure 7d) could be visualized by SEM (Figure S25), AFM (Figure 7e) and PLIM (Figure 7f). From the PLIM measurements, amplitude-weighted average photoluminescence decay lifetimes and spectra were read out (Figures S26–S28), confirming the uniform growth of SP **1B** from the termini of the seeds.

Hence, the evolution of extended metal-metal-interactions provides another feasible strategy to induce LSP. Although similar approaches have been applied for other metal complexes,[15–17,44] in these examples there was either no competition between metal-metal-interactions and H-bonding or the formation metal-metal-interactions was even overruled by the evolution of H-bonds. In our system, the growth of Pt···Pt-interactions drives the rearrangement of a strong, fourfold, all intermolecular H-bonding motif, ultimately enabling size control. As this LSP strategy is orthogonal to trapping by means of intramolecular H-bonding, we hypothesize that this could possibly give way to multiple kinetic trapping.[38]

Conclusion

In summary, we have achieved unique pathway-controllable metal-metal-interactions and MMLCT emission in a self-assembled Pt^{II} complex based on a non-preorganized, monodentate ligand design. Despite the widely known inability of square-planar complexes based on non-chelating ligands to undergo luminescence via meta-metal interactions, we demonstrate herein that this is indeed possible by rationally combining aromatic interactions with multiple hydrogen bonding to overrule the inherent steric effects of the metal coordination sphere. The bisamide motifs in the ligand backbone of complex **1** facilitate a rapid, kinetically controlled cooperative self-assembly into non-emissive H-type SP **1A** through fourfold H-bonding interactions. However, under thermodynamic conditions, a more efficient ligand coplanarization leads to superiorly stabilized SPs **1B** with extended Pt···Pt-interactions and remarkable ^{3}MMLCT luminescence with long lifetimes (up to 0.26 ms). Despite

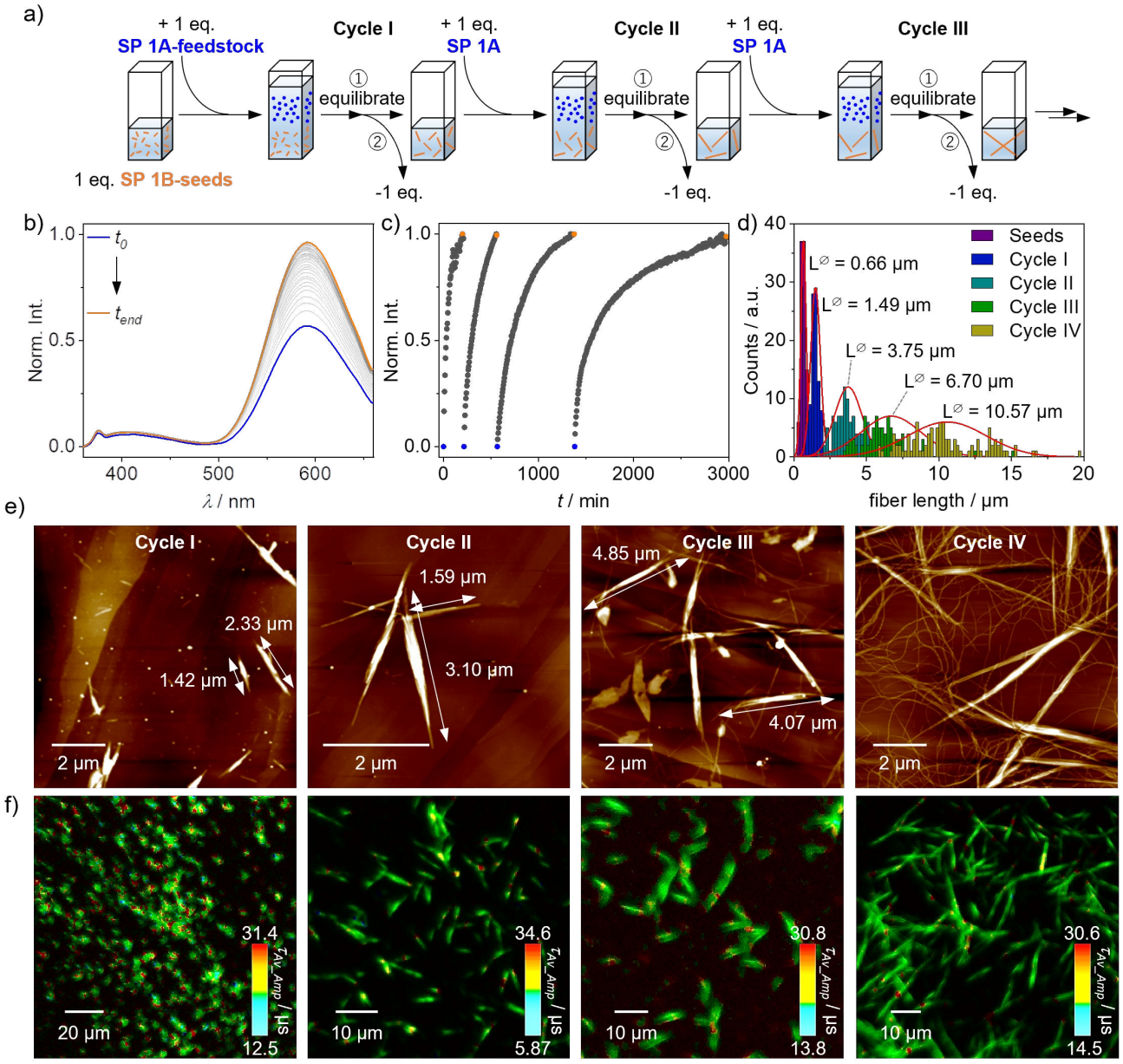

Figure 7. a) Schematic representation of the experimental procedure for the seed-mediated LSP. b) Time-dependent emission spectra after adding **1A** to seeds of **1B** ($c = 20$ µM, $T = 298$ K, MCH:$CHCl_3$ 7:3, $\lambda_{exc} = 333$ nm). c) Plot of the emission intensity against time during four LSP cycles ($\lambda = 593$ nm). d) Length distribution of the fibers after each cycle (lengths extracted from SEM images). AFM (e) and PLIM (f) images recorded after completion of each cycle ($\lambda_{exc} = 375$ nm).

the inability of **1** to generate intramolecularly H-bonded metastable monomers, seed-mediated LSP could be performed using SP **1A** as feedstock, driven by the formation of attractive Pt···Pt-interactions. The long emission lifetimes enabled us to use phosphorescence lifetime imaging (PLIM) as a new method to visualize and analyze the LSP growth of the emissive SPs with controlled length.

In our opinion, the accomplishment of MMLCT luminescence in materials that were previously observed to be non-emissive provides fundamental understanding of structure–property relationships in self-assembly and further broadens the fields of functional supramolecular materials and controlled SP.

Acknowledgements

We thank the VCI for a Kekulé fellowship (J.M.), the Alexander von Humboldt foundation for a postdoctoral scholarship (I.M.), the Deutsche Forschungsgemeinschaft (CRC 1450 inSight—431460824 and CRC 1459 intelligent matter—Project-ID 433682494) (J.M., G.F. and C.A.S.) as well as the DFG/L and NRW (INST 211/915-1 FUGG; DFG

EXC1003; C.A.S.). Open Access funding enabled and organized by Projekt DEAL.

Conflict of Interest

The authors declare no conflict of interest.

Data Availability Statement

The data that support the findings of this study are available in the Supporting Information of this article.

Keywords: supramolecular polymers · pathway complexity · luminescent assemblies · metal-metal-interactions · hydrogen bonding

[1] a) S. Datta, S. Takahashi, S. Yagai, *Acc. Mater. Res.* **2022**, *3*, 259; b) L. Brunsveld, B. J. B. Folmer, E. W. Meijer, R. P. Sijbesma, *Chem. Rev.* **2001**, *101*, 4071; c) G. Ghosh, A. Chakraborty, P. Pal, B. Jana, S. Ghosh, *Chem. Eur. J.* **2022**, *28*, e202201082; d) V. Saez Talens, J. Davis, C.-H. Wu, Z. Wen, F. Lauria, K. B. S. S. Gupta, R. Rudge, M. Boraghi, A. Hagemeijer, T. T. Trinh, P. Englebienne, I. K. Voets, J. I. Wu, R. E. Kieltyka, *J. Am. Chem. Soc.* **2020**, *142*, 19907; e) V. Saez Talens, D. M. M. Makurat, T. Liu, W. Dai, C. Guibert, W. E. M. Noteborn, I. K. Voets, R. E. Kieltyka, *Polym. Chem.* **2019**, *10*, 3146; f) S. Yagai, Y. Kitamoto, S. Datta, B. Adhikari, *Acc. Chem. Res.* **2019**, *52*, 1325; g) G. Ghosh, P. Dey, S. Ghosh, *Chem. Commun.* **2020**, *56*, 6757.

[2] N. Bäumer, J. Matern, G. Fernández, *Chem. Sci.* **2021**, *12*, 12248.

[3] a) D. Septiadi, A. Aliprandi, M. Mauro, L. de Cola, *RSC Adv.* **2014**, *4*, 25709; b) I. Maisuls, J. Singh, I. P. Salto, S. T. Steiner, T. M. Kirse, S. Niemann, C. A. Strassert, A. Faust, *Inorg. Chem.* **2021**, *60*, 11058; c) C. Ouyang, Y. Li, T. W. Rees, X. Liao, J. Jia, Y. Chen, X. Zhang, L. Ji, H. Chao, *Angew. Chem. Int. Ed.* **2021**, *60*, 4150; *Angew. Chem.* **2021**, *133*, 4196.

[4] Z. Li, Y. Han, Z. Gao, F. Wang, *ACS Catal.* **2017**, *7*, 4676.

[5] C.-H. Zhou, X. Zhao, *J. Organomet. Chem.* **2011**, *696*, 3322.

[6] C. Cebrián, M. Mauro, D. Kourkoulos, P. Mercandelli, D. Hertel, K. Meerholz, C. A. Strassert, L. de Cola, *Adv. Mater.* **2013**, *25*, 437.

[7] I. Maisuls, C. Wang, M. E. Gutierrez Suburu, S. Wilde, C.-G. Daniliuc, D. Brünink, N. L. Doltsinis, S. Ostendorp, G. Wilde, J. Kösters, U. Resch-Genger, C. A. Strassert, *Chem. Sci.* **2021**, *12*, 3270.

[8] V. W.-W. Yam, A. K.-W. Chan, E. Y.-H. Hong, *Nat. Chem. Rev.* **2020**, *4*, 528.

[9] V. W.-W. Yam, V. K.-M. Au, S. Y.-L. Leung, *Chem. Rev.* **2015**, *115*, 7589.

[10] W.-P. To, Q. Wan, G. S. M. Tong, C.-M. Che, *Trends Chem.* **2020**, *2*, 796.

[11] M. H.-Y. Chan, M. Ng, S. Y.-L. Leung, W. H. Lam, V. W.-W. Yam, *J. Am. Chem. Soc.* **2017**, *139*, 8639.

[12] V. C.-H. Wong, C. Po, S. Y.-L. Leung, A. K.-W. Chan, S. Yang, B. Zhu, X. Cui, V. W.-W. Yam, *J. Am. Chem. Soc.* **2018**, *140*, 657.

[13] M. E. Robinson, A. Nazemi, D. J. Lunn, D. W. Hayward, C. E. Boott, M.-S. Hsiao, R. L. Harniman, S. A. Davis, G. R. Whittell, R. M. Richardson, L. de Cola, I. Manners, *ACS Nano* **2017**, *11*, 9162.

[14] A. Aliprandi, M. Mauro, L. de Cola, *Nat. Chem.* **2016**, *8*, 10.

[15] G. Moreno-Alcántar, A. Aliprandi, R. Rouquette, L. Pesce, K. Wurst, C. Perego, P. Brüggeller, G. M. Pavan, L. de Cola, *Angew. Chem. Int. Ed.* **2021**, *60*, 5407; *Angew. Chem.* **2021**, *133*, 5467.

[16] Q. Wan, W.-P. To, X. Chang, C.-M. Che, *Chem* **2020**, *6*, 945.

[17] Q. Wan, W.-P. To, C. Yang, C.-M. Che, *Angew. Chem. Int. Ed.* **2018**, *57*, 3089; *Angew. Chem.* **2018**, *130*, 3143.

[18] N. Bäumer, K. K. Kartha, S. Buss, I. Maisuls, J. P. Palakkal, C. A. Strassert, G. Fernández, *Chem. Sci.* **2021**, *12*, 5236.

[19] M. E. Robinson, D. J. Lunn, A. Nazemi, G. R. Whittell, L. de Cola, I. Manners, *Chem. Commun.* **2015**, *51*, 15921.

[20] S. Chatnahalli Gangadharappa, I. Maisuls, I. P. Salto, S. Niemann, V. Bachtin, F. C. Herrmann, C. A. Strassert, *J. Phys. Chem. C* **2021**, *125*, 5739.

[21] C. A. Strassert, C.-H. Chien, M. D. Galvez Lopez, D. Kourkoulos, D. Hertel, K. Meerholz, L. de Cola, *Angew. Chem. Int. Ed.* **2011**, *50*, 946; *Angew. Chem.* **2011**, *123*, 976.

[22] M. Mydlak, M. Mauro, F. Polo, M. Felicetti, J. Leonhardt, G. Diener, L. de Cola, C. A. Strassert, *Chem. Mater.* **2011**, *23*, 3659.

[23] T.-F. Fu, L. Ao, Z.-C. Gao, X.-L. Zhang, F. Wang, *Chin. Chem. Lett.* **2016**, *27*, 1147.

[24] J. C. Y. Lin, S. S. Tang, C. S. Vasam, W. C. You, T. W. Ho, C. H. Huang, B. J. Sun, C. Y. Huang, C. S. Lee, W. S. Hwang, A. H. H. Chang, I. J. B. Lin, *Inorg. Chem.* **2008**, *47*, 2543.

[25] a) N. K. Allampally, M. J. Mayoral, S. Chansai, M. C. Lagunas, C. Hardacre, V. Stepanenko, R. Q. Albuquerque, G. Fernández, *Chem. Eur. J.* **2016**, *22*, 7810; b) N. Bäumer, K. K. Kartha, N. K. Allampally, S. Yagai, R. Q. Albuquerque, G. Fernández, *Angew. Chem. Int. Ed.* **2019**, *58*, 15626; *Angew. Chem.* **2019**, *131*, 15772; c) L. Herkert, P. Selter, C. G. Daniliuc, N. Bäumer, J. P. Palakkal, G. Fernández, M. R. Hansen, *Chem. Eur. J.* **2021**, *27*, 4617.

[26] a) Y. Han, Z. Gao, C. Wang, R. Zhong, F. Wang, *Coord. Chem. Rev.* **2020**, *414*, 213300; b) X.-D. Xu, J. Zhang, L.-J. Chen, X.-L. Zhao, D.-X. Wang, H.-B. Yang, *Chem. Eur. J.* **2012**, *18*, 1659.

[27] P. A. Korevaar, S. J. George, A. J. Markvoort, M. M. J. Smulders, P. A. J. Hilbers, A. P. H. J. Schenning, T. F. A. de Greef, E. W. Meijer, *Nature* **2012**, *481*, 492.

[28] a) N. Bäumer, K. K. Kartha, S. Buss, J. P. Palakkal, C. A. Strassert, G. Fernández, *Org. Chem. Front.* **2021**, *8*, 4138; b) L. Straub, D. González-Abradelo, C. A. Strassert, *Chem. Commun.* **2017**, *53*, 11806.

[29] a) H. M. M. ten Eikelder, A. J. Markvoort, T. F. A. de Greef, P. A. J. Hilbers, *J. Phys. Chem. B* **2012**, *116*, 5291; b) A. J. Markvoort, H. M. ten Eikelder, P. A. Hilbers, T. F. de Greef, E. W. Meijer, *Nat. Commun.* **2011**, *2*, 509.

[30] Y. Tidhar, H. Weissman, S. G. Wolf, A. Gulino, B. Rybtchinski, *Chem. Eur. J.* **2011**, *17*, 6068.

[31] I. Helmers, N. Bäumer, G. Fernández, *Chem. Commun.* **2020**, *56*, 13808.

[32] J. Matern, Y. Dorca, L. Sánchez, G. Fernández, *Angew. Chem. Int. Ed.* **2019**, *58*, 16730; *Angew. Chem.* **2019**, *131*, 16884.

[33] J. Matern, Z. Fernandez, N. Bäumer, G. Fernandez, *Angew. Chem. Int. Ed.* **2022**, *61*, e202203783; *Angew. Chem.* **2022**, *134*, e202203783.

[34] E. E. Greciano, S. Alsina, G. Ghosh, G. Fernández, L. Sánchez, *Small Methods* **2020**, *4*, 1900715.

[35] E. E. Greciano, M. A. Martínez, S. Alsina, A. Laguna, L. Sánchez, *Org. Chem. Front.* **2021**, *8*, 5328.

[36] a) J. S. Nowick, M. Abdi, K. A. Bellamo, J. A. Love, E. J. Martinez, G. Noronha, E. M. Smith, J. W. Ziller, *J. Am. Chem. Soc.* **1995**, *117*, 89; b) S. H. Gellman, G. P. Dado, G. B. Liang, B. R. Adams, *J. Am. Chem. Soc.* **1991**, *113*, 1164.

[37] S. Ogi, V. Stepanenko, J. Thein, F. Würthner, *J. Am. Chem. Soc.* **2016**, *138*, 670.
[38] H. Choi, S. Ogi, N. Ando, S. Yamaguchi, *J. Am. Chem. Soc.* **2021**, *143*, 2953.
[39] E. E. Greciano, L. Sánchez, *Chem. Eur. J.* **2016**, *22*, 13724.
[40] S. Ogi, V. Stepanenko, K. Sugiyasu, M. Takeuchi, F. Würthner, *J. Am. Chem. Soc.* **2015**, *137*, 3300.
[41] a) A. Jamadar, A. K. Singh, L. Roy, A. Das, *J. Mater. Chem. C* **2021**, *9*, 11893; b) K. K. Kartha, N. K. Allampally, A. T. Politi, D. D. Prabhu, H. Ouchi, R. Q. Albuquerque, S. Yagai, G. Fernández, *Chem. Sci.* **2019**, *10*, 752.
[42] A. Chakraborty, G. Ghosh, D. S. Pal, S. Varghese, S. Ghosh, *Chem. Sci.* **2019**, *10*, 7345.
[43] M. Wehner, F. Würthner, *Nat. Chem. Rev.* **2020**, *4*, 38.
[44] K. Zhang, M. C.-L. Yeung, S. Y.-L. Leung, V. W.-W. Yam, *Proc. Natl. Acad. Sci. USA* **2017**, *114*, 11844.
[45] Q. Wan, J. Xia, W. Lu, J. Yang, C.-M. Che, *J. Am. Chem. Soc.* **2019**, *141*, 11572.
[46] a) S. Ogi, K. Sugiyasu, S. Manna, S. Samitsu, M. Takeuchi, *Nat. Chem.* **2014**, *6*, 188; b) T. Gädt, N. S. Ieong, G. Cambridge, M. A. Winnik, I. Manners, *Nat. Mater.* **2009**, *8*, 144; c) X. Wang, G. Guerin, H. Wang, Y. Wang, I. Manners, M. A. Winnik, *Science* **2007**, *317*, 644.

Manuscript received: June 8, 2022
Accepted manuscript online: June 24, 2022
Version of record online: August 17, 2022